

Nuclear Quantum Effects Induce Metallization of Dense Solid Molecular Hydrogen

Sam Azadi*

*Department of Materials Science and Thomas Young Center,
Imperial College London, London SW7 2AZ, United Kingdom*

Ranber Singh

Department of Physics, Sri Guru Gobind Singh College, Sector 26, 160019 Chandigarh, India

T. D. Kühne

*Department of Chemistry and Paderborn Center for Parallel Computing,
University of Paderborn, Warburger Str. 100, D-33098 Paderborn,
Germany Institute for Lightweight Design with Hybrid Systems,
Warburger Str. 100, D-33098 Paderborn, Germany*

(Dated: September 28, 2018)

We present an accurate computational study of the electronic structure and lattice dynamics of solid molecular hydrogen at high pressure. The band-gap energies of the $C2/c$, Pc , and $P6_3/m$ structures at pressures of 250, 300, and 350 GPa are calculated using the diffusion quantum Monte Carlo (DMC) method. The atomic configurations are obtained from ab-initio path-integral molecular dynamics (PIMD) simulations at 300 K and 300 GPa to investigate the impact of zero-point energy and temperature-induced motion of the protons including anharmonic effects. We find that finite temperature and nuclear quantum effects reduce the band-gaps substantially, leading to metallization of the $C2/c$ and Pc phases via band overlap; the effect on the band-gap of the $P6_3/m$ structure is less pronounced. Our combined DMC-PIMD simulations predict that there are no excitonic or quasiparticle energy gaps for the $C2/c$ and Pc phases at 300 GPa and 300 K. Our results also indicate a strong correlation between the band-gap energy and vibron modes. This strong coupling induces a band-gap reduction of more than 2.46 eV in high-pressure solid molecular hydrogen. Comparing our DMC-PIMD with experimental results available, we conclude that none of the structures proposed is a good candidate for phases III and IV of solid hydrogen.

I. INTRODUCTION

Determining the metallization pressure of solid hydrogen is one of the great challenges of high-pressure physics. Since 1935, when it was predicted that molecular solid hydrogen would become a metallic atomic crystal at 25 GPa¹, compressed hydrogen has been of huge scientific interest. Additional interest arises from the possible existence of room-temperature superconductivity², a metallic liquid ground state³, and the relevance of solid hydrogen to astrophysics^{4,5}.

Early spectroscopic measurements at low temperature suggested the existence of three phases^{4,6}. Phase I, which is stable up to 110 GPa, is a molecular solid composed of quantum rotors arranged in a hexagonal close-packed structure. Changes in the low-frequency regions of the Raman and infrared (IR) spectra imply the existence of phase II, also known as the broken-symmetry phase, above 110 GPa. The appearance of phase III at 150 GPa is accompanied by a large discontinuity in the Raman spectrum and a strong rise in the spectral weight of the molecular vibrons. Phase IV, characterized by the two vibrons in its Raman spectrum, was discovered at 300 K and pressures above 230 GPa⁷⁻⁹. Recently, another new phase has been claimed to exist at pressures above 200 GPa and higher temperatures (e.g. 480 K at 255 GPa)¹⁰. This phase is thought to meet phases I and IV at a triple point, near which hydrogen retains

its molecular character. The most recent experimental results indicate that H₂ and hydrogen deuteride (HD) at 300 K and pressures greater than 325 GPa transform into a new phase V that is characterized by substantial weakening of the vibrational Raman activity¹¹. Other features include a change in the pressure dependence of the fundamental vibrational frequency and partial loss of the low-frequency excitations.

Although it is very difficult to reach the static pressure of more than 400 GPa at which hydrogen is normally expected to metallize, some experimental results have been interpreted as indicating metallization at room temperature below 300 GPa⁷. However, other experiments show no evidence of the optical conductivity expected of a metal at any temperature up to the highest pressures explored¹². Experimentally, it remains unclear whether or not the molecular phases III and IV are metallic, although it has been suggested that phase V may be non-molecular (atomic) and metallic¹¹. Metallization is believed to occur either via the dissociation of hydrogen molecules and a structural transformation to an atomic metallic phase^{7,13}, or by band-gap closure within the molecular phase^{14,15}. The mechanism and origin of band-gap closure are not well-known.

The electronic structure of solid molecular hydrogen have mainly been investigated by means of density-functional theory (DFT)-based methods¹⁶⁻²⁵, as well as using the quasiparticle (QP) approach^{15,26}. Although DFT-based methods are usually able to describe the crys-

tal structures and relative total energies of the relevant phases, their insufficiencies are more apparent in the case of band-gap calculations²⁷. To obtain precise energy gaps, it is vital to go beyond mean-field theories and solve the many-electron Schrödinger equation directly. In this work, we combine two sophisticated methods, diffusion quantum Monte Carlo (DMC) and path-integral molecular dynamics (PIMD), to calculate the excitonic and quasiparticle band-gaps of dense hydrogen at both zero and room temperature.

The DMC method is one of the most accurate known techniques for evaluating the total energies of systems of more than a few tens of interacting quantum particles^{28–30}. It has been indicated recently that DMC can provide an accurate description of the phase diagram of solid molecular hydrogen³¹. Although the DMC method was originally designed to study the electronic ground state, it is also capable of providing accurate information about excited states in atoms, molecules, and crystals^{32–35}. In general, DMC calculations of excitations in crystals remain challenging because of the $1/N$ effect: The fractional change in the total energy due to the presence of a one- or two-particle excitation is inversely proportional to the number of electrons in the simulation cell. Since large simulation cells are required to provide an accurate description of the infinite solid, high-precision calculations are necessary³⁶.

Structures of crystalline materials are normally determined by x-ray or neutron diffraction methods. These techniques are very challenging for elements with low atomic numbers such as hydrogen, which is part of the reason the structures of phases III and IV have remained uncertain. Fortunately, even though the crystal structures are still unknown, optical phonon modes disappear, appear, or experience discrete shifts when the crystal structure changes. It is, therefore, possible to identify the transitions between phases using optical methods.

The main input to any DMC calculation is the structure of the system under study, which, in this case, is unknown. Hence, there is no option but to use structures predicted by mean-field theories such as DFT. It is now generally accepted that DFT results for high-pressure hydrogen critically depends on the choice of exchange-correlation (XC) functional^{21,22,25}. This frustrating limitation may be the main cause of the contradictions between different theoretical results^{37,38}.

In the present work, we carry out a comprehensive study of the band-gap energy of high-pressure solid molecular hydrogen at zero and finite temperature. We concentrate on the smallest band-gap, which may be direct or indirect, of the $C2/c$, Pc , and $P6_3/m$ structures. These include all of the candidates suggested by DFT calculations for phases III and IV^{16–19,31}.

II. COMPUTATIONAL DETAILS

We considered the $C2/c$, Pc , and $P6_3/m$ crystal structures of solid molecular hydrogen at $P = 250, 300,$ and 350 GPa. According to previously conducted DFT simulations, the $C2/c$ and Pc structures are the most favorable candidates for phase III and phase IV^{16,17,31}, respectively. All structures, which were afterwards used for our DMC simulations, were first fully relaxed at constant pressure at the DFT level. The latter calculations were carried out within the pseudopotential and plane-wave approach using the Quantum Espresso suite of programs³⁹. All DFT calculations employed a dense $16 \times 16 \times 16$ \mathbf{k} -point mesh, norm-conserving pseudopotentials, a plane-wave basis set with a cutoff of 100 Ry, as well as the Becke-Lee-Yang-Parr (BLYP) generalized gradient approximation to the exact XC functional⁴⁰. In our recent work⁴¹, we have demonstrated that for studying the high-pressure solid hydrogen phase diagram, the BLYP XC functional is more accurate than most other semi-local XC functionals. Independent studies of others have confirmed the superior accuracy of the employed BLYP XC functional for the description of thermodynamic properties of high-pressure hydrogen^{22,31,42}. Geometry and cell optimizations were performed using the Broyden-Fletcher-Goldfarb-Shanno quasi-Newton algorithm with a convergence thresholds on the total energy and forces of 0.01 mRy and 0.1 mRy/Bohr, respectively, to guarantee convergence of the total energy to better than 1 meV/proton and the pressure to better than 0.1 GPa/proton.

Our DMC simulations were conducted using the CASINO QMC code⁴³ and a trial function of the Slater-Jastrow (SJ) form,

$$\Psi_T(\mathbf{R}) = \exp[J(\mathbf{R})] \det[\psi_n(\mathbf{r}_i^\uparrow)] \det[\psi_n(\mathbf{r}_j^\downarrow)], \quad (1)$$

where \mathbf{R} is a $3N$ -dimensional vector that defines the positions of all N electrons, \mathbf{r}_i^\uparrow is the position of the i th spin-up electron, \mathbf{r}_j^\downarrow is the position of the j th spin-down electron, $\exp[J(\mathbf{R})]$ is the Jastrow correlation factor, whereas $\det[\psi_n(\mathbf{r}_i^\uparrow)]$ and $\det[\psi_n(\mathbf{r}_j^\downarrow)]$ are Slater determinants of spin-up and spin-down one-electron orbitals, respectively. The one-electron orbitals were also obtained from the DFT calculations using the plane-wave Quantum Espresso code³⁹. However, to guarantee converge to the complete basis set limit, a rather large basis set cutoff of 200 Ry was chosen⁴⁴. Thereafter, the plane-wave orbitals were transformed into a blip polynomial basis⁴⁵.

As is customary, our QMC calculations were carried out using finite simulation cells subject to periodic boundary conditions which introduce finite-size (FS) errors. An important contribution to the FS errors in our calculations arises from the treatment of the Coulomb potential energy. The Coulomb interaction is inconsistent with the periodicity of the simulation cell and has to be replaced by the Ewald interaction, which is the Green's function of Poisson's equation subject to peri-

odic boundary conditions. Unlike the Coulomb interaction, the Ewald interaction depends on the size and shape of the simulation cell. Therefore, we employed canonical twist averaging to correct single-particle FS errors which are analogous to \mathbf{k} -point sampling errors in DFT⁴⁶. Specifically, we performed twist-averaged DMC calculations based on eight randomly chosen twists at three different system sizes for each phase and volume. We used 192, 432, and 648 atoms in our simulation cells for the $C2/c$ phase, which has 24 atoms in the primitive unit cell, 192, 384, and 576 atoms for the Pc structure with 48 atoms in the primitive unit cell, and 28, 288, and 768 hydrogen atoms for the $P6_3/m$ phase that has 16 atoms in the primitive unit cell.

We linearly extrapolated the twist-averaged energy per atom to the thermodynamic limit in order to correct for many-body FS errors, which are due to the long range of both the Coulomb interaction and the two-body correlations. We verified that the linear fitting is accurate, because the finite-size error in the energy per atom decreases as $1/N$, where N is the number of particles in the simulation cell.

Our Jastrow correlation factor consists of a polynomial one-body electron-nucleus (1b), two-body electron-electron (2b), three body electron-electron-nucleus (3b), as well as plane-wave expansions in the electron-electron separation (p)⁴⁷. We found that the latter p term makes significant improvements to the wave function and the variational energy, since it describes the long-range correlation term in the Jastrow, which plays an important role in our calculations. The parameters within the Jastrow were optimized by means of variance minimization at the variational quantum Monte Carlo (VMC) level^{48,49}.

The QP energy gap is defined as

$$\Delta_{\text{qp}} = E_{N+1} + E_{N-1} - 2E_0, \quad (2)$$

where E_{N+1} [E_{N-1}] is the many-body total energy of the system after an electron has been added [removed from] the system, while E_0 is the ground-state energy. Our calculations of Δ_{qp} were performed at the Γ -point of the supercell Brillouin zone, equivalent to a mesh of k -points in the primitive Brillouin zone. Technical details of the QP calculations are given in our recent work⁴¹. We created excitonic states by promoting an electron from a valence-band orbital into a conduction-band state with the same wave vector. However, the so created states do not cover all excitonic effects since no configuration interactions are taken into account. The absorption gap to an excitonic state at Γ is

$$\Delta_{\text{exc}} = E' - E_0, \quad (3)$$

where E' and E_0 are the total energies of the first excited and the ground state as obtained by DMC. We found that the difference between the triplet and singlet excitonic gaps is small in the systems studied here. For example, in the case of the $C2/c$ structure at 250 GPa, the singlet-triplet splitting is 0.2(1) eV. We focus, therefore, on singlet excitonic absorption gaps.

Finite-temperature second generation Car-Parrinello PIMD simulations were performed to account for harmonic and anharmonic zero-point motion (ZPM)^{50–52}. The combined path-integral generalized Langevin (PIGLET) scheme of Ceriotti et al. was employed here⁵³, as implemented in the i-Pi wrapper⁵⁴, to reduce the number of computationally expensive imaginary-time replicas.

Eventually, convergence was achieved with as few as six imaginary-time replicas. All of the simulations were performed using the isobaric-isothermal (NPT) ensemble at 300 K and 300 GPa. The interatomic forces were computed at the DFT level using the Quantum Espresso suite of programs and a plane-wave cutoff of 680 eV. The simulations consisted of 96 protons for the $C2/c$ and Pc phases and 128 atoms for the $P6_3/m$ structure. The first Brillouin zone was sampled using a $2 \times 2 \times 2$ Monkhorst-Pack k -point mesh⁵⁵. In each case, 25 statistically independent configurations, which are separated by 1 ps, were considered to compute the associated ensemble averages at the DMC level. Since for each PIMD configuration the DMC energy is obtained based on eight randomly chosen twists²⁶, in total $3 \times 25 \times 8 = 600$ DMC simulations have been performed to obtain reliable results.

III. RESULTS AND DISCUSSION

The free energy difference between two phases at constant temperature and pressure is $\Delta G = \Delta H - T\Delta S$, where $\Delta H = \Delta E + P\Delta V$. Herein, G, H, T, S, E, P and V are the Gibbs free energy, enthalpy, temperature, entropy, internal energy, pressure and volume of the system. We calculated the ensemble average of the enthalpy $\langle H \rangle = N^{-1}\sum_{i=1}^N H_i$, where H_i is the enthalpy of the system at each configuration. Thus, the enthalpy difference between two phases can be defined as $\langle \Delta H \rangle = \langle H_2 \rangle - \langle H_1 \rangle$. In Fig. 1, $\langle H \rangle$ for the $C2/c$, Pc , and $P6_3/m$ phases at room temperature and 300 GPa are shown. The resulting difference $\langle \Delta H \rangle$ between the $C2/c$ and Pc structures is about 2(1) meV/atom, while it is 0.23(2) eV/atom between the $P6_3/m$ and the two other phases. However, at constant temperature, ΔS between the $C2/c$ and Pc phases is less than 10 meV/atom³¹. This suggests that ΔS is the dominant term within ΔG for the $C2/c$ to Pc transition and that this is an entropy driven transition. Assuming that ΔS is relatively similar for all considered structures, this also suggests that, at room temperature and 300 GPa, the Gibbs free energy of $P6_3/m$ is much lower than that of the $C2/c$ and Pc phases, respectively.

A. Electronic Density of States

We investigated the electronic structure of the $C2/c$, Pc , and $P6_3/m$ by computing the averaged DOS at room temperature and 300 GPa, which is shown in Fig. 2. As

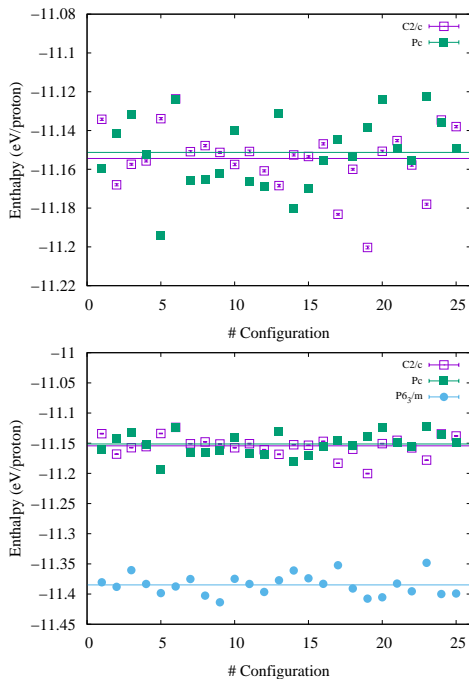


FIG. 1. DMC enthalpies of 25 statistically independent configurations obtained by *ab-initio* PIMD simulation at $P=300$ GPa and $T=300$ K. The ensemble averaged energy is illustrated by a flat line.

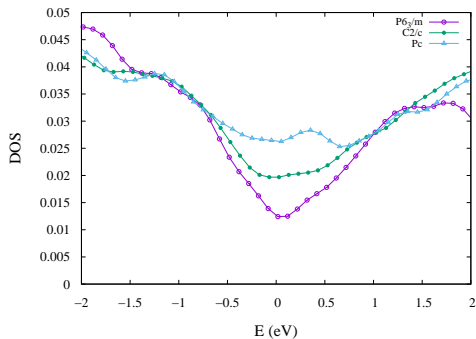


FIG. 2. Ensemble averaged DOS per particle as obtained by *ab-initio* PIMD simulations at $P=300$ GPa and $T=300$ K for the $C2/c$, Pc , and $P6_3/m$ phases. The Fermi energy is located at $E=0$. All energies and DOS are in eV and eV^{-1} , respectively.

can be seen, the electronic DOS at Fermi level of the $P6_3/m$ phase is smaller than that of the $C2/c$ and Pc structures. Nevertheless, at the DFT level, all of the considered phases obey metallic behavior.

B. Band-gap Energy

In a recent paper we reported our QP and excitonic band-gap results at the nuclear ground state, where the ZPM and temperature-induced vibrations of the protons are neglected⁴¹. Therein, we found that the exci-

ton binding energy is smaller than 100 meV/atom and that our DMC QP and excitonic band-gaps are within error bars to one another. Therefore, in this work, we do not attempt to distinguish the excitonic from the QP band-gap. Instead, by calculating the static-nucleus energy band-gaps using DMC, we quantify the many-body corrections to the band structure that are absent in the mean-field DFT approach. Although these contributions are relatively independent of lattice vibrations and temperature, it is well known that nuclear quantum effects are significant in hydrogen-rich systems and greatly affect the metallization of high-pressure solid hydrogen²¹. Assuming the validity of the Born-Oppenheimer approximation, the full electron-nuclear wave function $\Psi(\mathbf{R}, \mathbf{d})$ can be approximated in the form $\Phi(\mathbf{R}|\mathbf{d})\chi(\mathbf{d})$, where $\Phi(\mathbf{R}|\mathbf{d})$ is a function of the positions $\mathbf{R} = (\mathbf{r}_1, \mathbf{r}_2, \dots, \mathbf{r}_N)$ of the N electrons in the supercell at fixed nuclear positions \mathbf{d} , while $\chi(\mathbf{d})$ is the nuclear wave function. The measured band structure is then an average of the band structures calculated from $\Phi(\mathbf{R}|\mathbf{d})$, which are weighted according to the nuclear probability density. We sampled the nuclear probability density by performing finite-temperature PIMD simulations using DFT within the generalized gradient approximation in order to take harmonic and anharmonic nuclear quantum and finite-temperature effects into account.

It is not straightforward to measure the band-gap at pressures greater than 300 GPa, but experimental results suggest that solid hydrogen is indeed an insulator in this pressure range^{8,12,18}. It is, therefore, reasonable to assume that the $C2/c$, Pc , and $P6_3/m$ structures all have non-zero band-gaps at 300 GPa and 300 K. Based on this assumption, we treat each PIMD configuration as an insulator and calculate the DFT band structure of that configuration by occupying the same number of one-electron DFT orbitals at every wave vector in the simulation cell Brillouin zone. Using this protocol, we found that the highest occupied and lowest unoccupied states belong to different \mathbf{k} -points and that the difference between them, which we denote as the dynamic gap, is negative for almost every nuclear configuration sampled. This implies that, at the DFT level, the nuclear quantum and finite-temperature effects render all the studied structures metallic.

To correct for the underestimation of the dynamic gap by DFT, we introduce a *scissor operator*. The dynamic DFT band-gap is increased from E_g^{DFT} to $E_g^{DFT} + \delta_{sci}$, where $\delta_{sci} = E_g^{DMC} - E_g^{DFT}$ is calculated for a perfect crystalline supercell at the static level⁴¹. The scissor operator depends on the crystal structure and the pressure applied. However, a detailed study and the specific values of δ_{sci} for all the studied structures at $P = 250, 300,$ and 350 GPa are reported in our recent work⁴¹. The resulting scissor-corrected dynamic band-gaps of the $C2/c$, Pc , and $P6_3/m$ structures at room temperature and a pressure of 300 GPa are shown in Fig. 3. We find that the harmonic and anharmonic ZPM and finite-temperature contributions are substantial, and that the $C2/c$ and Pc

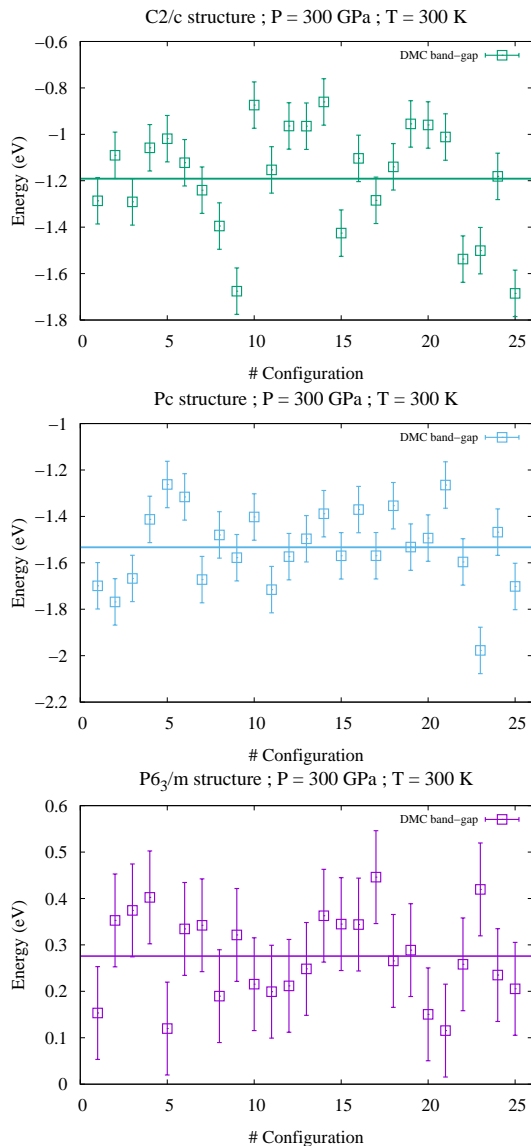


FIG. 3. Energy band-gaps of the $C2/c$, Pc , and $P6_3/m$ structures at room temperature and a pressure of 300 GPa. The horizontal lines denotes the corresponding ensemble averaged band-gap energies. A DMC scissor operator is used to correct the DFT energy band-gaps. The statistical uncertainties within the band-gap as obtained by the present DMC calculations are indicated by vertical bars. The occurrence of negative band-gaps is due to the fact that the valence band maximum (VBM) and conduction band minimum (CBM), which occur at different \mathbf{k} -points, do overlap.

structures remain metallic even after the scissor correction has been applied. The scissor-corrected static band-gaps of the $C2/c$, Pc , and $P6_3/m$ structures at 300 GPa, which are calculated by DMC, are 2.3(2), 2.4(2), and 2.8(2) eV, respectively⁴¹. The inclusion of nuclear quantum and finite-temperature effects lowers the $C2/c$, Pc , and $P6_3/m$ band-gaps by as much as 3.4(2), 3.8(2), and 2.5(2) eV, respectively, relative to static-nucleus results.

Discussion

Our results indicate a strong structure dependence of the protons ZPM and thermal contributions. The $C2/c$ and Pc crystal structures have weakly bonded graphene-like layers, while three-quarters of the H_2 molecules in the $P6_3/m$ phase lie flat within the plane and a quarter lie perpendicular to the plane. The centers of the molecules fall on a slightly distorted hexagonal close-packed lattice¹⁶. The quantum and thermal vibrational motions increase the intermolecular interactions and weaken the intramolecular bonding, an effect that appears to be more significant for the $C2/c$ and Pc structures than for the $P6_3/m$ phase. The high structural flexibility of phase IV at pressures of 250–350 GPa and temperatures of 300–500 K has also been observed in a previous *ab initio* variable-cell MD simulations, which found that the protons in the graphene-like layers can readily transfer to neighboring molecular sites via a simultaneous rotation of three-molecule rings⁵⁶. Our results confirm that this behavior has a strong effect on the band-gaps of the $C2/c$ and Pc structures.

According to our band-gap energy results, the $C2/c$ and Pc structures, thought to be the best candidates for phases III and IV of solid molecular hydrogen³¹, are metallic at room temperature and 300 GPa, in disagreement with most of the experimental evidence. Another possible crystal structure, $Pbcn$, entails two different layers of graphene-like three-molecule rings with elongated and unbound H_2 molecules¹⁶. Assuming that the reduction of the band-gap due to the proton motion in $Pbcn$ is similar to that in Pc , we would also expect $Pbcn$ to be metallic at room temperature and 300 GPa. There is some experimental evidence of metallization of high-pressure hydrogen at room temperature and pressures around 300 GPa⁷, but the onset of metallic behavior was thought to be accompanied by a first-order structural transition, presumably into a monatomic liquid state.

There are experimental band-gap results up to a pressure of 350 GPa^{8,12,18}. The optical transmission spectrum of phase IV shows an overall increase of absorption and a band-gap reduction to 1.8 eV at 315 GPa⁸. According to these results, metallization of solid hydrogen at and below room temperature should happen at pressures above 350 GPa. This scenario appears to contradict our band-gap energy results for the $C2/c$ and Pc phases. Assuming that the experimental measurements of the band-gaps are accurate, our analysis implies that the $C2/c$ and Pc phases are unlikely candidates for high-pressure solid molecular hydrogen at room temperature and 300 GPa. Instead, it is more likely that the $C2/c$ and Pc structures become semi-metallic at pressures between 250 to 300 GPa.

The dynamic band-gap of the $P6_3/m$ phases at room temperature and 300 GPa is larger than the that of the $C2/c$ and Pc structures. The static DMC band-gap of the $P6_3/m$ phase is also larger than that of the other layered-structures. In addition, the band-gap reduction,

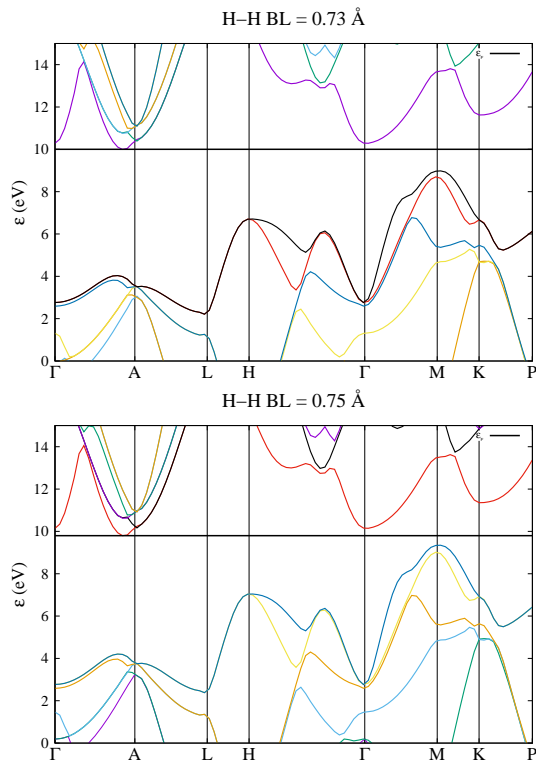


FIG. 4. Electronic band structure of the $P6_3/m$ structure at fixed volume. The DFT results are obtained for two intramolecular H–H bond-lengths (BL) of 0.73 and 0.75 Å, respectively. The location of the Fermi level is indicated by the black horizontal line.

due to ZPM and temperature contributions, is in the $P6_3/m$ phase ~ 1 eV smaller than in the two other structures studied. Experimental Raman spectra, however, suggest that phase IV consists of two different graphene-like sheets and unbound H_2 molecules⁸. The metallic nature of the $C2/c$ and Pc structures leads us to doubt that any graphene-like structure with weak interactions between layers remains an insulator at room temperature and 300 GPa, so this interpretation of the Raman data

is difficult to reconcile with the existence of a band-gap. It seems likely that the true structures of phase III and phase IV of high-pressure hydrogen remain unknown¹⁰.

To gain a deeper understanding of this problem, we studied the correlation between the electronic band structure and the intramolecular H–H bond-length. For that purpose, we performed band structure calculations for the $P6_3/m$ phase, which has the largest band-gap, at fixed volume and two intramolecular H–H bond-lengths (BL) of 0.73 and 0.75 Å (Fig. 4), respectively. We found a strong coupling between the highest-occupied state and the intramolecular H–H BL. The gradient of the energy gap with respect to the intramolecular BL is ~ 27.3 eV/Å, and is independent of XC functional⁴¹. Since the root mean vibration amplitude of a H_2 molecule due to the vibron modes is ~ 0.09 Å^{57–60}, the band-gap reduction caused by ZP vibrations is ~ 2.46 eV, which is in excellent agreement with the 2.5(2) eV band-gap reduction obtained by our PIMD calculations.

IV. CONCLUSION

To summarize, based on combined *ab-initio* PIMD and DMC simulations, we find that finite-temperature and nuclear quantum effects leads to a band-gap reduction of at least 2.5 eV. Since this renders all candidate structures we have considered here metallic, which is in contrast with available experimental measurements, we conclude that none of the proposed structures are likely candidates for phase III and IV of solid molecular hydrogen.

The authors would like to thank the Gauss Center for Supercomputing (GCS) for providing computing time through the John von Neumann Institute for Computing (NIC) on the GCS share of the supercomputer JUQUEEN at the Jülich Supercomputing Centre (JSC). Additional computing facilities were provided through the DECI-13 PRACE project QMCBENZ15 and the Dutch national supercomputer Cartesius. This project has received funding from the European Research Council (ERC) under the European Union’s Horizon 2020 research and innovation programme (grant agreement No 716142).

* s.azadi@imperial.ac.uk

¹ E. Wigner and H. B. Huntington, J. Chem. Phys. **3**, 764 (1935).

² N. W. Ashcroft, Phys. Rev. Lett **21**, 1748 (1968).

³ S. A. Bonev, E. Schwegler, T. Ogitsu, and G. Galli, Nature **431**, 669 (2004).

⁴ H. K. Mao and R. J. Hemley, Rev. Mod. Phys. **66**, 671 (1994).

⁵ V. L. Ginzburg, Phys. Usp. **42**, 353 (1999).

⁶ I. F. Silvera, Rev. Mod. Phys. **52**, 393 (1980).

⁷ M. I. Eremets and I. A. Troyan, Nat. Mater. **10**, 927 (2011).

⁸ R. T. Howie, C. L. Guillaume, T. Scheler, A. F. Goncharov, and E. Gregoryanz, Phys. Rev. Lett. **108**, 125501 (2012).

⁹ R. T. Howie, I. B. Magdau, A. F. Goncharov, G. J. Ackland, and E. Gregoryanz, Phys. Rev. Lett. **113**, 175501 (2014).

¹⁰ R. T. Howie, P. Dalladay-Simpson, and E. Gregoryanz, Nat. Mater. **14**, 495 (2015).

¹¹ P. Dalladay-Simpson, R. T. Howie, and E. Gregoryanz, Nature **529**, 63 (2016).

¹² C. S. Zha, Z. Liu, and R. J. Hemley, Phys. Rev. Lett. **108**, 146402 (2012).

¹³ S. Azadi, B. Monserrat, W. M. C. Foulkes, and R. J. Needs,

- Phys. Rev. Lett. **112**, 165501 (2014).
- ¹⁴ M. Städele and R. Martin, Phys. Rev. Lett. **84**, 6070 (2000).
 - ¹⁵ K. A. Johnson and N. W. Ashcroft, Nature **403**, 632 (2000).
 - ¹⁶ C. J. Pickard and R. J. Needs, Nat. Phys. **3**, 473 (2007).
 - ¹⁷ C. J. Pickard, M. Martinez-Canales, and R. J. Needs, Phys. Rev. B **85**, 214114 (2012).
 - ¹⁸ A. F. Goncharov, J. S. Tse, H. Wang, J. Yang, V. V. Struzhkin, R. T. Howie, and E. Gregoryanz, Phys. Rev. B **87**, 024101 (2013).
 - ¹⁹ I. B. Magdău and G. J. Ackland, Phys. Rev. B **87**, 174110 (2013).
 - ²⁰ I. I. Naumov, R. E. Cohen, and R. J. Hemley, Phys. Rev. B **88**, 045125 (2013).
 - ²¹ M. A. Morales, J. M. McMahon, C. Pierleoni, and D. M. Ceperley, Phys. Rev. B **87**, 184107 (2013).
 - ²² R. C. Clay, J. Mcminis, J. M. McMahon, C. Pierleoni, D. M. Ceperley, and M. A. Morales, Phys. Rev. B **89**, 184106 (2014).
 - ²³ S. Azadi and T. D. Kühne, JETP Lett. **95**, 449 (2012).
 - ²⁴ R. Singh, S. Azadi, and T. D. Kühne, Phys. Rev. B **90**, 014110 (2014).
 - ²⁵ S. Azadi and W. M. C. Foulkes, Phys. Rev. B **88**, 014115 (2013).
 - ²⁶ S. Azadi, W. M. C. Foulkes, and T. D. Kühne, New J. Phys. **15**, 113005 (2013).
 - ²⁷ J. P. Perdew, A. Ruzsinszky, L. A. Constantin, J. Sun, , and G. I. Csonka, J. Chem. Theory Comput. **5**, 902 (2009).
 - ²⁸ D. M. Ceperley and B. J. Alder, Phys. Rev. Lett. **45**, 566 (1980).
 - ²⁹ W. M. C. Foulkes, L. Mitas, R. J. Needs, and G. Rajagopal, Rev. Mod. Phys. **73**, 33 (2001).
 - ³⁰ S. Azadi, R. Singh, and T. D. Kühne, Int. J. Quantum Chem. **115**, 1673 (2015).
 - ³¹ N. D. Drummond, B. Monserrat, J. H. Lloyd-Williams, P. L. Rios, C. J. Pickard, and R. J. Needs, Nat. Comm. **6**, 7794 (2015).
 - ³² L. Mitas and R. M. Martin, Phys. Rev. Lett. **72**, 2438 (1994).
 - ³³ A. J. Williamson, R. Q. Hood, R. J. Needs, and G. Rajagopal, Phys. Rev. B **57**, 12140 (1998).
 - ³⁴ M. D. Towler, R. Q. Hood, and R. J. Needs, Phys. Rev. B **62**, 2330 (2000).
 - ³⁵ N. D. Drummond, R. J. Needs, A. Sorouri, and W. M. C. Foulkes, Phys. Rev. B **78**, 125106 (2008).
 - ³⁶ S. Azadi and T. D. Kühne, J. Chem. Phys. **146**, 084503 (2017).
 - ³⁷ J. McMinis, R. C. Clay, D. Lee, and M. A. Morales, Phys. Rev. Lett. **114**, 105305 (2015).
 - ³⁸ J. M. McMahon, M. A. Morales, C. Pierleoni, and D. M. Ceperley, Rev. Mod. Phys. **84**, 1607 (2012).
 - ³⁹ P. Giannozzi and *et al.*, J. Phys.: Condens. Matt. **21**, 395502 (2009).
 - ⁴⁰ C. Lee, W. Yang, and R. G. Parr, Phys. Rev. B **37**, 785 (1988).
 - ⁴¹ S. Azadi, N. Drummond, and W. M. C. Foulkes, Phys. Rev. B **95**, 035142 (2017).
 - ⁴² R. C. Clay III, M. Holzmann, D. M. Ceperley, and M. A. Morales, Phys. Rev. B **93**, 035121 (2016).
 - ⁴³ R. J. Needs, M. D. Towler, N. D. Drummond, and P. L. Rios, J. Phys.: Condens. Matt. **22**, 023201 (2010).
 - ⁴⁴ S. Azadi, C. Cavazzoni, and S. Sorella, Phys. Rev. B **82**, 125112 (2010).
 - ⁴⁵ D. Alfè and M. J. Gillan, Phys. Rev. B **70**, 161101(R) (2004).
 - ⁴⁶ C. Lin, F. H. Zong, and D. M. Ceperley, Phys. Rev. E **64**, 016701 (2001).
 - ⁴⁷ N. D. Drummond, M. D. Towler, and R. J. Needs, Phys. Rev. B **70**, 235119 (2004).
 - ⁴⁸ C. J. Umrigar, K. G. Wilson, and J. W. Wilkins, Phys. Rev. Lett. **60**, 1719 (1988).
 - ⁴⁹ N. D. Drummond and R. J. Needs, Phys. Rev. B **72**, 085124 (2005).
 - ⁵⁰ T. D. Kühne, M. Krack, F. R. Mohamed, and M. Parrinello, Phys. Rev. Lett. **98**, 066401 (2007).
 - ⁵¹ T. D. Kühne, WIREs Comput. Mol. Sci. **4**, 391 (2014).
 - ⁵² C. John, T. Spura, S. Habershon, and T. D. Kühne, Phys. Rev. E **93**, 043305 (2016).
 - ⁵³ M. Ceriotti and D. E. Manolopoulos, Phys. Rev. Lett. **109**, 100604 (2012).
 - ⁵⁴ M. Ceriotti, J. More, and D. E. Manolopoulos, Comput. Phys. Commun. **185**, 1019 (2014).
 - ⁵⁵ H. J. Monkhorst and J. D. Pack, Phys. Rev. B **13**, 5188 (1976).
 - ⁵⁶ H. Liu and Y. Ma, Phys. Rev. Lett. **110**, 025903 (2013).
 - ⁵⁷ V. Labet, P. Gonzalez-Morelos, R. Hoffmann, and N. W. Ashcroft, J. Chem. Phys. **136**, 074501 (2012).
 - ⁵⁸ V. Labet, R. Hoffmann, and N. W. Ashcroft, J. Chem. Phys. **136**, 074502 (2012).
 - ⁵⁹ V. Labet, R. Hoffmann, and N. W. Ashcroft, J. Chem. Phys. **136**, 074503 (2012).
 - ⁶⁰ V. Labet, R. Hoffmann, and N. W. Ashcroft, J. Chem. Phys. **136**, 074504 (2012).